

Composite Stretchable Sensors for the Detection of Asymmetric Deformations in a Soft Manipulator

David Hardman¹, Ryman Hashem¹ and Fumiya Iida¹

Abstract—As the task-complexities demanded of soft robots continue to increase, so too does the need for soft sensorized skins which can provide complex tactile feedback. Here we consider the detection of asymmetric deformations by designing and validating an easy-to-fabricate hydrogel-silicone composite sensor for deployment in an underactuated soft robotic manipulator. For proprioception and exteroception, this skin can sense asymmetric bifurcations in a stretchable skin without affecting functionality. Our method facilitates the sensor’s use in a wide range of soft robotic actuators: we present its ability to respond to repeated, incremental, and oscillating stimuli in the soft manipulator, and demonstrate its ease of integration into a closed-loop control system. We experimentally find the sensors capable of withstanding over 200% strain before the onset of delamination.

I. INTRODUCTION

The fast-growing field of soft robotics has led to the emergence of biomimetic actuators which can be deployed into hostile environments, work safely alongside humans, and manipulate delicate objects, such as foodstuffs [1]. To integrate these developments into fully soft and compliant robotic systems, soft and flexible sensors must also be incorporated [2], using customizable sensor morphologies to return detailed information about the nonlinear continuum deformations of the actuators and their environments.

Typically, elastomer-based sensing techniques for soft robots are based on the incorporation of piezoelectric conductive fillers into silicones, which can be cast or injection moulded [3], [4], [5]. Where custom sensor morphologies are required, fibrous sensors or liquid channels can be embedded into a surrounding elastomer matrix [6], [7], [8]. Alternatively, piezoelectric conductive filaments can be used in conjunction with fused deposition modelling [9]. However, such approaches often introduce delamination failure mechanisms due to interfacial stresses between the different stiffness materials.

The highly stretchable nature of hydrogels and their tunable compositions makes them an appealing choice for soft robotics [10], [11] and soft sensors [12], [13], [14], [15]. Their encasement in silicone has been found to yield stretchable sensors with low hysteresis [16], [17]. Gelatin-based actuators have been explored for their ease of fabrication, biocompatibility, and edibility [18], [19], [20]. Their low melting point enables straightforward extrusion-based printing [21], [22], aiding the manufacture of custom strain sensors using conductive additives [23], [24].

¹D. Hardman, R. Hashem, and F. Iida are with the Department of Engineering, University of Cambridge, UK dsh46@cam.ac.uk

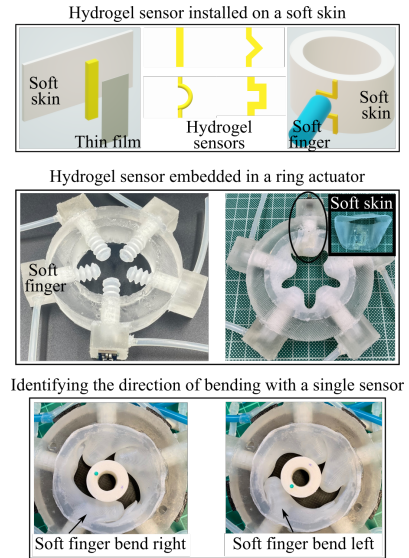


Fig. 1: Embedding the composite skin into a soft manipulator, where it senses the bifurcation direction and object collisions of a soft finger.

In this work, we propose a soft composite sensor which can be straightforwardly fabricated from an ionically sensorized self-healing gelatin/glycerol hydrogel and a platinum-catalyzed silicone, widely used in soft robotic manufacture. By coupling the two low-stiffness materials, we demonstrate how the strain sensors can reliably and repeatably respond to strains of at least 200% before delamination occurs. Our approach benefits from the hydrogel’s extrudability, which enables the straightforward manufacture of custom morphologies.

We characterize the behavior of our composite sensor (Fig. 1) and highlight its use in the design and development of custom morphologies using a soft manipulator (Fig. 1) [25]. As demonstrated in the authors’ previous work [26], this multi-degree-of-freedom actuator can be used to facilitate in-hand manipulation of small objects. The system’s underactuation means that additional sensors are required to detect the direction and magnitude of the finger deformations. Previous iterations have used two sensorized thermoplastic filaments to detect the bifurcation direction, but their limited stretchability was found to limit the actuator’s performance and lead to rapid delamination [26]. By using the same actuator, we show that a single composite channel significantly outperforms the two filament sensors from [26] in detecting asymmetric deformations, whilst operating well below the

delamination threshold.

After some tests to determine suitable geometries (Section II-B) and morphologies (Section II-C) for the asymmetric sensors, we incorporate the sensorized skin into the actuator (Section II-D), where it is shown to clearly and repeatedly respond to out of plane deformations and asymmetries, significantly outperforming the two filament sensors presented in [26]. In the manipulator, we demonstrate how a single channel (Fig. 1) detects finger positions, bifurcation directions, and object collisions without impeding the motion of the actuator, and how sensor measurements can be fed back to the controller for closed-loop decision making.

II. RESULTS AND DISCUSSION

A. Composite Material

Fig. 2c shows the design of a test sample: A sensorized gelatin/glycerol hydrogel channel of $w \times t$ mm is cast onto the 1 mm thick soft skin and is enclosed using a thin silicone layer (Section IV). Once cured, Figs. 2a & 2b shows the response of the 4×2 mm channel to applied strain trapezoids of 300%. The stretchable composite withstands and responds clearly and repeatably to the significant deformations, drifting only 0.009 V over the 4 repetitions (less than 3% of the average response magnitude). No overshoot is noticeable in the sensor responses, though small levels of material relaxation are apparent during unloading. When the signals are converted to resistances, the sensor responses contain clearly nonlinear regions at higher strains. This contrasts with the highly linear responses of the unconstrained hydrogel in previous studies [22], suggesting that the interfacial forces acting between the hydrogel and its soft casing cause a shift in the composite material's response at higher strains. Without this casing, the unenclosed channel quickly delaminates from the soft skin (see accompanying video), whilst the enclosed channel can continually undergo applied strain cycles. In addition, the silicone holds the hydrogel in place if the damage is inflicted, such that an applied heat source can be used to heal the internal hydrogel without a loss of morphology, as demonstrated in Fig. 2d and the accompanying video. In this example, both the hydrogel and silicone are cut with a scalpel so that the sensor stops responding. A rework station's air gun is then used to heat the sensor in the area of damage locally, facilitating healing of the hydrogel. The composite remains weakened, since the silicone does not heal, but this heat source is sufficient to recover the sensitivity to 50% strains: a property that could be used to temporarily deal with a damaged soft robot until the sensor is fully repaired.

B. Characterizing Sensor Geometries

Before comparing sensor morphologies, a suitable geometry for the hydrogel channel is briefly selected: Fig. 3 tests 9 combinations of w & t values from Fig. 2c. Each is longitudinally tested with 30% strain trapezoids, over which the response is approximately linear. The sensitivity is calculated:

$$\frac{R_{30} - R_0}{R_0}. \quad (1)$$

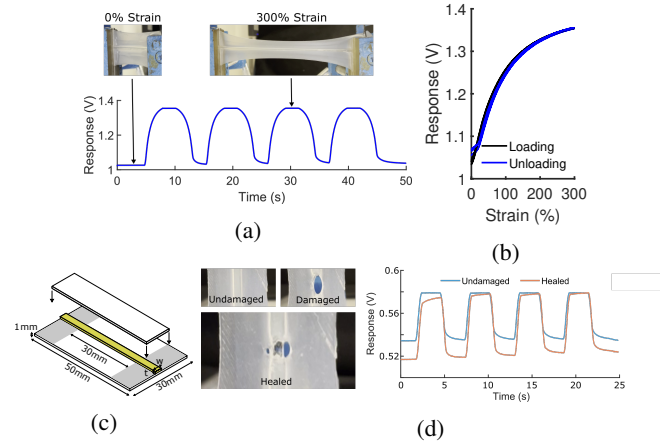


Fig. 2: a-b) Response of the 4×2 mm sensorized sample to applied strains of 300%, plotted with time (a) and strain (b). Note the non-zero y-intercept. c) A sensorized hydrogel strip (yellow) is sandwiched between soft skin and a thin silicone layer to create each test sample. d) Healing of the sensorized hydrogel through applied heat. Though the encasing soft skin does not heal, it holds the broken hydrogel channels together during heating.

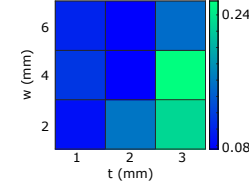


Fig. 3: Sensitivities of the geometries during 30% trapezoidal tests: 4×3 mm & 2×3 mm demonstrate the highest values.

All nine sensors give clean and repeatable responses to the strain trapezoids, withstanding strains of over 200% before delamination. This is due to the similar stress responses: both materials require a stress of approximately 0.6 MPa to produce a maximum 450% strain [22], [27]. They are thus all mechanically suitable for integration with the ring actuator, and we select the 4×3 mm channel based on its highest observed sensitivity. Though the trend of Fig. 3 suggests that greater t values would further increase the measured sensitivity, 3 mm is taken to be the maximum before the actuator's function is affected. Significant thicknesses should not be added to the actuator's skin since the channels might affect manipulation tasks or get caught more easily and initiate delamination. Wider channels would impact the composite sensor's ability to detect asymmetric deformations (Section II-C).

C. Characterizing Asymmetric Deformations

Sensorized skins for Section I's soft actuator must be capable of detecting deformations perpendicular to the plane of the sensor, and discerning their direction through an asymmetric response. Fig. 4a simulates these deformations using a similarly sized probe fastened to a robotic arm. We expect vertical deformations - A & B represent depressions

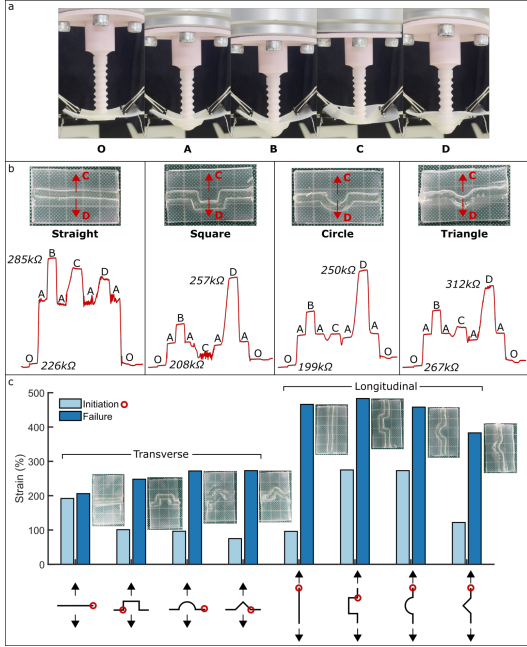


Fig. 4: a) Longitudinal morphology responses. A probe applies out-of-plane/asymmetric deformations. b) The responses of the longitudinal morphologies, with the asymmetric directions indicated. c) Strain values at which the longitudinal and transverse sensors begin delamination and undergo complete failure. Red circles indicate initiation sites.

of 10 & 15 mm, respectively - to be easily detectable via the channel's piezo resistive response. Indeed, the response of a straight longitudinal sensor in Fig. 4b demonstrates a marked difference in the measured resistances between positions O, A, & B, confirming the material's ability to detect these deformations.

However, this straight sensor morphology cannot discern the direction of asymmetric deformations (directions C & D in Fig. 4b, representative of the actuator's bifurcation directions), due to the symmetry of the sensorized strip; peaks C & D in the sensor's response are of very similar magnitude, despite representing displacements in opposite directions. To add directionality information, asymmetries are introduced into the longitudinal sensor: Fig. 4 shows these new morphologies, referred to as square, circle, and triangle. Dimensions of each are given in Section IV. Fig. 4 plots their responses to identical deformations (accompanying video), where the difference between positions C & D is much clearer; the deformation in the direction of the additional material results in a significant resistance increase. The additional material means that purely vertical displacements produce a proportionally lesser response than the straight line, since the global strain increase is not as high. Still, deformations A & B produce clear responses in all tested samples. The square morphology is the only sample that decreases resistance after moving from A → C; for the triangle, a slight increase occurs, whilst the stabilized values at A & C are very similar for the circle. Therefore,

the square is the best choice for distinguishing between the two directions: at these representative deformations, the two respond with opposite signs and significantly different magnitude.

To ensure that the shapes do not quickly delaminate, Fig. 4c shows the results of tensile tests for each of the four sensor morphologies, on samples cast both transversely and longitudinally. The sites at which delamination initiates are indicated on all - this always occurs either at the clamped edge, or at a cast corner: the greatest stress concentrations. However, the square morphology does not cause any earlier failure than the other morphologies. Its additional material causes it to outlast the straight morphology to final failure. The square, circle, and triangle longitudinal morphologies do not stop functioning as sensors until $\geq 300\%$ strain.

D. Integration into Actuator

Based on the results of Section II-C, a 4×3 mm hydrogel channel with square morphology is embedded into the skin of the soft actuator (Fig. 5). For this preliminary demonstration of the composite sensor's asymmetric capabilities, we detect the deformations of only one finger: in scaling the system, all five responses could be used alongside the applied pressure signals to infer the manipulator's state.

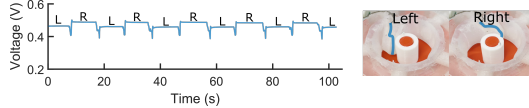
Fig. 5 validates the sensor's ability to detect the finger's deformations with much higher precision than that of the two filament sensors [26]. In 5a, the plot shows the capability of the single sensor morphology to detect asymmetries, as designed. The extended finger is manually oscillated between the left & right bistable states when a cylinder of 17.5 mm diameter is centred in the actuator: the sensor can clearly distinguish between the two, and repeatably settles to raw voltages of 0.459 V & 0.487 V, respectively. Sharp decreases in resistance characterize the transition between the states, as the finger is forced backwards and the skin's strain is reduced.

In Figs. 5b & 5c, the cylinder is removed and the finger is actuated radially. Firstly, the pressure is switched between 0 kPa & 50 kPa. The response quickly stabilizes when the state is switched, with no overshoots and negligible drift during the measured period. As the hydrogel maintains environmental equilibrium over longer time periods, the baseline (0 kPa) resistance is expected to drift; however, the local repeatability demonstrated here means that a brief application of known pressure values is sufficient to recalibrate the sensor. Similarly, in Fig. 5c, 10 kPa steps are applied, and the difference in response between each is clearly distinguishable. The radial displacements of the finger for each pressure are presented in Table I, which also includes 8 negative pressures to draw the finger into the body of the actuator.

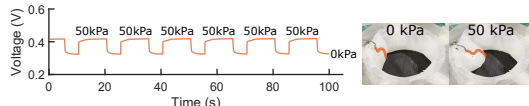
Fig. 6 uses this full range of available pressures during 10 triangular waves, mapping these to the resistive response of the finger. The unloading response is roughly linear, whilst the loading curve demonstrates more hysteresis: still, the proximity of the two curves suggests that applied pressure can be easily estimated from individual resistance values.

TABLE I: Radial displacements of the finger in Figs. 5b, 5c, & 6 over the range of applied pressures.

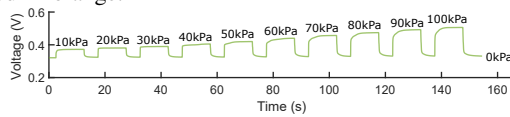
Pressure (kPa)	-80	-70	-60	-50	-40	-30	-20	-10	0	10	20	30	40	50	60	70	80	90	100
Displacement (mm)	8	9	9.5	9.5	9.5	10.5	12	13	13.5	14.5	16	17.5	18.5	19.5	20.5	21.5	22.5	23	23.5



(a) Asymmetric deformations. The position of the hydrogel channel is marked in blue.



(b) Repeated deformations. The position of the hydrogel channel is marked in orange.



(c) Applied pressures of increasing magnitude.

Fig. 5: Sensorizing one of the manipulator's fingers with a soft skin. a) Bifurcations around a cylinder. The finger is manually switched between the bistable states, which are individually identified by the sensor. b) With no cylinder, a pressure of 50 kPa is repeatedly applied to the finger. c) With no central cylinder, pressures between 10 & 100 kPa are applied to the finger in 10 kPa increments.

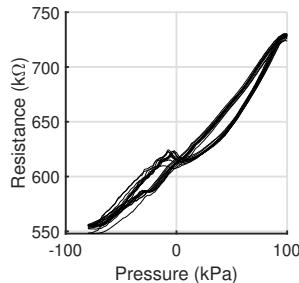
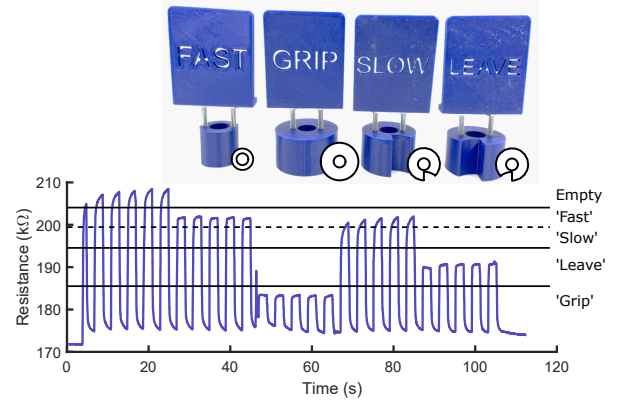


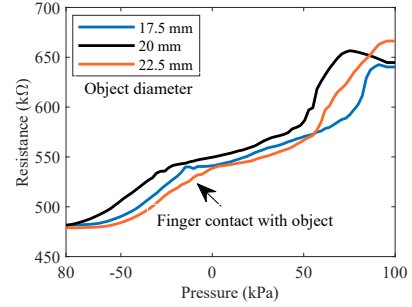
Fig. 6: The single finger's resistive response vs applied pressure, over 10 cycles of applied $-80 \rightarrow 100$ kPa triangular waves.

A kink in the response is seen during the transition from negative to positive applied pressure, where the hysteresis loops intersect, which is due to the skin's freedom of movement in the unpressurized state.

Fig. 5 has demonstrated the proprioceptive capabilities of the composite sensor application, without considering the presence of differently shaped objects which impart external forces during the actuation. We next consider exteroceptive sensing in the manipulator: Figure 7a proposes a closed-loop setup in which the shape of a manipulated object is used to determine the subsequent control pattern. 4 cases are used: a 20 mm cylinder which should be quickly rotated; a 35 mm cylinder which should be gripped by all 5 fingers; a 30 mm



(a) Closed-loop control signal.



(b) Fine-scale cylindrical exteroception.

Fig. 7: a) Closed-loop control: based on the size and asymmetry of the sign detected, the actuator adjusts its actuation pattern. b) Finer-scale exteroception: small changes in object diameter can be detected by analysing the shape of the sensor's transient response.

cylinder with an asymmetric cutout which should be slowly rotated; and a mirror image of the slow cylinder which should not be actuated. The asymmetric cutouts force the sensorized finger to deflect leftwards or rightwards, allowing the two to be distinguished by the controller. Fig. 7a shows the sensor response as the empty case and 4 objects are probed with the finger. For the majority of cases, it is straightforward to define thresholds which can categorize the objects. However, the fast & slow cases have similar magnitudes, and external effects such as the manipulator's orientation would also be expected to shift the thresholded values. A more robust categorization must therefore rely on the transient response of the signal as it reaches steady state: the fast sign stabilizes much more quickly than the asymmetric deformation. The accompanying video shows the closed-loop manipulation in progress - the finger checks each object twice before deciding on the actuation pattern.

Such transient response analyses can be used for finer-scale exteroception: Fig 7b shows how a linearly-applied pressure ramp elicits different sensor responses for cylinders

of 17.5, 20.0, & 22.5 mm diameter. Though the response magnitudes are similar, the pressures at which they occur varies based on the pressure at which the cylinder is contacted and moved. In this way, the raw sensor data can be used to infer the interaction with objects as well as empty-case proprioception for more complex closed-loop control sequences. If particular objects or deformations are known, the composite sensor's straightforward fabrication allows matching morphologies to quickly be customized and designed, enabling clear categorization.

III. CONCLUSIONS

This work introduces a composite sensor consisting of a sensorized hydrogel channel encased in a silicone skin. It can repeatably and reliably respond to strain whilst remaining soft, stretchable, and flexible. The ability to cast or extrude both components introduces a significant level of customizability, enabling a range of sensor morphologies to be fabricated, including those designed to detect asymmetric deformations. The encasing of the hydrogel channel prevents delamination under repeated strain cycles, protects the hydrogel from fluctuations in environmental conditions, and maintains sensor morphologies during healing. The sensors frequently undergo strains of over 200% before the onset of delamination.

To illustrate the customizability which our composite sensors provide, we demonstrate both proprioceptive and exteroceptive sensing in the skin of a soft manipulator. In the longitudinal configuration, an asymmetric square morphology is shown to undergo 275% applied strain before the delamination, demonstrating its potential to be incorporated into a large range of soft robotic actuators without risk. The composite excellently detects the motions of the soft actuator, showing distinctions between both bifurcation states and 11 different pressure values during radial deformation. Notably, we present our preliminary findings of the use of transient analysis to extract the state of the underactuated manipulator, enabling closed-loop control. Further work will seek to extract these transient effects by training a neural network to recognize the different transient states and constant values, aiming to identify the shapes of different objects by combining the information from multiple sensors. This couples machine learning techniques with morphology-level optimization in order to infer significant levels of proprioceptive and exteroceptive data from simple sensor implementations.

IV. MATERIALS AND METHODS

All characterization samples are fabricated from a combination of platinum-catalyzed silicone (Ecoflex 0030 and Slacker with a mix ratio of 1:0.5, Smooth-On) and a sensorized gelatin/glycerol hydrogel. The composition of the ionically sensorized gelatin/glycerol hydrogel is taken from the authors' previous work [22], and is mixed in the mass ratio 1:1.5:2.5:0.2:0.1 Ge:Gl:H₂O:CA:NaCl, where Ge → 240/260 pork gelatin powder (*Cake SOS*), Gl → glycerol (*Fisher Scientific*), CA → citric acid monohydrate (*Fisher*

Scientific), and NaCl → sodium chloride-based table salt (*Sainsbury's*). Cold water is first poured onto the gelatin powder in a glass beaker and left to bloom for 10 minutes before Gl, CA, & NaCl are added. The beaker is covered with parafilm to minimize evaporation, and transferred to a 50°C water bath. Once the mixture homogenizes, the bath is used to maintain the sol state for casting: the sol-gel transition occurs at ~45°C. After casting, the hydrogel loses water to reach an environmental equilibrium, where it remains flexible and stretchable: all cast samples are left for at least 24 hours before encasing/testing in order to facilitate this. Once cured, the hydrogel behaves as a strain sensor, linearly increasing its resistance as a unidirectional strain is applied.

To fabricate the composites, silicone is first cast into a 50×30×1 mm mould, which is 3D printed from polylactic acid (PLA). After curing, a hydrogel strip is cast onto its free surface at 50°C, using a PLA pattern (t mm thickness) to mask the areas which should not be sensorized. This pattern is either longitudinal (the sensorized strip covers the entire 50 mm length) or transverse (the 30 mm length, matching the width of the soft actuator's skin). The sample is left for 24 hours at room temperature before the pattern is removed, and a thin layer of silicone is cast to encase the hydrogel strip (Fig. 2c). By encasing the hydrogel in silicone, the bond between the two materials is significantly improved compared to a simple two-layer composite, as can be seen in the accompanying video. When measuring the resistance of a sample, silver conductive yarn is sewn through the sensorized channel 5 mm from its edges, which is connected to the measurement circuit.

To implement the sensor in the soft skin of the ring actuator, a similar method of casting the soft skin, sensor, and the thin film is accomplished. The sensor is centred and placed in front of a soft finger. The fabrication procedure of the ring actuator is followed similar to the authors' previous work [25]. Briefly, each cap of the soft fingers is glued with the soft skin with silicone glue (sil-poxy, Smooth-On). To control the soft fingers, we used the same setup provided in [25], [26].

Alternating current (AC) impedances are measured with a 100 kHz sampling rate, using a *National Instruments* USB-6212 multifunction I/O device. A 10 kHz sine wave between ±2 V is applied across a potential divider, with one side of the sensor connected to the ground and a matched resistor joining this to the USB-6212's output, such that an increase in the sensor's resistance results in an increased peak-to-peak measurement at the measured node. In Fig. 4's morphology tests, 680 kΩ is used; and during the actuator's characterization (Fig. 5), this is 160 kΩ. All plotted responses are the upper envelope of the measured response, smoothed using a 1000-sample rolling window. Before measurements are taken, a shorted circuit is analyzed to approximate a 272 Ω background resistance in the setup. Since this is negligible compared to the ~10⁵ Ω measured responses, this is not considered further. Fig. 7a's response is measured using a *Keysight E4980AL LCR Meter* at 100 kHz, which sends measured resistances directly to the PC which controls the

actuator.

Tensile tests are performed by clamping 10 mm of each sample's ends. One clamp is secured to the table, whilst the other is attached to a *Universal Robots UR5* robot arm, programmed to move only in the vertical axis. Strain values are calculated from the 30 mm unstressed length. All trapezoids are applied at 30 mms^{-1} , whilst uniaxial failure tests use a quasistatic 5 mms^{-1} rate. Initiation is taken to occur at the first visible evidence of fracture or delamination, whilst failure is defined as the point at which the sample no longer functions as a strain sensor, whether due to delamination of the soft skin/hydrogel bond or total fracture of the specimen.

Out-of-plane deformation tests of the longitudinal sensors (Fig. 4a & b) are performed using a UR5 arm equipped with a 3D printed PLA end effector (Fig. 4). The 6 mm diameter probe is covered with one of the ring actuator's bellows in order to replicate the deformations expected during integration with the actuator. Positions A & B represent vertical deformations of 10 & 15 mm, respectively, whilst positions C & D start at position A and rotate 0.1 radians about an axis 167.5 mm above the longitudinal sensor, which drags the centre transversely along a 17.65 mm arc length. 2 s pauses are implemented between each move, with motion limits of 50 mms^{-1} and 100 mms^{-2} . Asymmetric morphologies are cast with a 4×3 mm channel passing through a point transversely offset by 7.5 mm from the centre of the 50 mm length. All are straight for the first 17.5 mm from either end, necessitating a semicircle of radius 7.5 mm, a 'triangle' of side length 10.6 mm, and a rectangle with side lengths 15 mm and 7.5 mm.

ACKNOWLEDGEMENTS

This work was supported by the SHERO project, a Future and Emerging Technologies (FET) programme of the European Commission (grant agreement ID 828818), and by EPSRC's RoboPatient EP/T00519X/1 and EP/R513180/1 DTP.

AUTHOR DISCLOSURE STATEMENT

The authors declare no competing interests.

REFERENCES

- [1] D. Rus and M. T. Tolley, "Design, fabrication and control of soft robots," *Nature*, vol. 521, no. 7553, pp. 467–475, 2015.
- [2] M. Amjadi, K.-U. Kyung, I. Park, and M. Sitti, "Stretchable, skin-mountable, and wearable strain sensors and their potential applications: a review," *Advanced Functional Materials*, vol. 26, no. 11, pp. 1678–1698, 2016.
- [3] C. Mattmann, F. Clemens, and G. Tröster, "Sensor for measuring strain in textile," *Sensors*, vol. 8, no. 6, pp. 3719–3732, 2008.
- [4] A. Georgopoulou and F. Clemens, "Piezoresistive Elastomer-Based Composite Strain Sensors and Their Applications," *ACS Applied Electronic Materials*, vol. 2, no. 7, pp. 1826–1842, 2020.
- [5] S. Sareh, A. Jiang, A. Faragasso, Y. Noh, T. Nanayakkara, P. Dasgupta, L. D. Seneviratne, H. A. Wurdemann, and K. Althoefer, "Bio-inspired tactile sensor sleeve for surgical soft manipulators," in *2014 IEEE International Conference on Robotics and Automation (ICRA)*, pp. 1454–1459, IEEE, 2014.
- [6] Y.-L. Park, B.-R. Chen, and R. J. Wood, "Design and fabrication of soft artificial skin using embedded microchannels and liquid conductors," *IEEE Sensors journal*, vol. 12, no. 8, pp. 2711–2718, 2012.
- [7] R. K. Kramer, C. Majidi, R. Sahai, and R. J. Wood, "Soft curvature sensors for joint angle proprioception," in *2011 IEEE/RSJ International Conference on Intelligent Robots and Systems*, pp. 1919–1926, IEEE, 2011.
- [8] A. Georgopoulou, S. Michel, and F. Clemens, "Sensorized robotic skin based on piezoresistive sensor fiber composites produced with injection molding of liquid silicone," *Polymers*, vol. 13, no. 8, 2021.
- [9] T. Hainsworth, L. Smith, S. Alexander, and R. MacCurdy, "A Fabrication Free, 3D Printed, Multi-Material, Self-Sensing Soft Actuator," *IEEE Robotics and Automation Letters*, vol. 5, no. 3, pp. 4118–4125, 2020.
- [10] H. Banerjee, M. Suhail, and H. Ren, "Hydrogel actuators and sensors for biomedical soft robots: brief overview with impending challenges," *Biomimetics*, vol. 3, no. 3, p. 15, 2018.
- [11] Y. Lee, W. Song, and J.-Y. Sun, "Hydrogel soft robotics," *Materials Today Physics*, vol. 15, p. 100258, 2020.
- [12] P. He, J. Wu, X. Pan, L. Chen, K. Liu, H. Gao, H. Wu, S. Cao, L. Huang, and Y. Ni, "Anti-freezing and moisturizing conductive hydrogels for strain sensing and moist-electric generation applications," *Journal of Materials Chemistry A*, vol. 8, no. 6, pp. 3109–3118, 2020.
- [13] G. Cai, J. Wang, K. Qian, J. Chen, S. Li, and P. S. Lee, "Extremely stretchable strain sensors based on conductive self-healing dynamic cross-links hydrogels for human-motion detection," *Advanced Science*, vol. 4, no. 2, p. 1600190, 2017.
- [14] Y.-J. Liu, W.-T. Cao, M.-G. Ma, and P. Wan, "Ultrasensitive wearable soft strain sensors of conductive, self-healing, and elastic hydrogels with synergistic "soft and hard" hybrid networks," *ACS applied materials & interfaces*, vol. 9, no. 30, pp. 25559–25570, 2017.
- [15] Z. Shao, X. Hu, W. Cheng, Y. Zhao, J. Hou, M. Wu, D. Xue, and Y. Wang, "Degradable self-adhesive epidermal sensors prepared from conductive nanocomposite hydrogel," *Nanoscale*, 2020.
- [16] Z. Shen, Z. Zhang, N. Zhang, J. Li, P. Zhou, F. Hu, Y. Rong, B. Lu, and G. Gu, "High-stretchability, ultralow-hysteresis conducting polymer hydrogel strain sensors for soft machines," *Advanced Materials*, p. 2203650, 8 2022.
- [17] Z. Sun, S. Wang, Y. Zhao, Z. Zhong, and L. Zuo, "Discriminating soft actuators' thermal stimuli and mechanical deformation by hydrogel sensors and machine learning," *Advanced Intelligent Systems*, p. 2200089, 7 2022.
- [18] J. Shintake, H. Sonar, E. Piskarev, J. Paik, and D. Floreano, "Soft pneumatic gelatin actuator for edible robotics," in *2017 IEEE/RSJ International Conference on Intelligent Robots and Systems (IROS)*, pp. 6221–6226, IEEE, 2017.
- [19] M. Baumgartner, F. Hartmann, M. Drack, D. Preninger, D. Wirthl, R. Gerstmayr, L. Lehner, G. Mao, R. Pruckner, S. Demchyshyn, L. Reiter, M. Strobel, T. Stockinger, D. Schiller, S. Kimeswenger, F. Greibich, G. Buchberger, E. Bradt, S. Hild, S. Bauer, and M. Kaltenbrunner, "Resilient yet entirely degradable gelatin-based biogels for soft robots and electronics," *Nature Materials*, vol. 19, no. 10, pp. 1102–1109, 2020.
- [20] M. K. A. Heiden, D. Preninger, L. Lehner, M. Baumgartner, M. Drack, E. Woritzka, D. Schiller, R. Gerstmayr, F. Hartmann, "3D-printing of resilient biogels for omnidirectional and exteroceptive soft actuators," *Science Robotics*, vol. 2119, no. February, pp. 1–11, 2022.
- [21] D. Hardman, J. Hughes, T. G. Thuruthel, K. Gilday, and F. Iida, "3d printable sensorized soft gelatin hydrogel for multi-material soft structures," *IEEE Robotics and Automation Letters*, 2021.
- [22] D. Hardman, T. George Thuruthel, and F. Iida, "Self-healing ionic gelatin/glycerol hydrogels for strain sensing applications," *NPG Asia Materials*, vol. 14, 2022.
- [23] J. T. Muth, D. M. Vogt, R. L. Truby, Y. Mengüç, D. B. Kolesky, R. J. Wood, and J. A. Lewis, "Embedded 3d printing of strain sensors within highly stretchable elastomers," *Advanced materials*, vol. 26, no. 36, pp. 6307–6312, 2014.
- [24] R. L. Truby and J. A. Lewis, "Printing soft matter in three dimensions," *Nature*, vol. 540, no. 7633, pp. 371–378, 2016.
- [25] R. Hashem, S. Kazemi, M. Stommel, L. K. Cheng, and W. Xu, "A biologically inspired ring-shaped soft pneumatic actuator for large deformations," *Soft Robotics*, 2021.
- [26] R. Hashem and F. Iida, "Embedded soft sensing in soft ring actuator for aiding with the self-organisation of the in-hand rotational manipulation," *IEEE International Conference on Soft Robotics 2022 (RoboSoft'22)*, 2022.
- [27] N. Ni and L. Zhang, "Dielectric elastomer sensors," in *Elastomers* (N. Cankaya, ed.), ch. 11, Rijeka: IntechOpen, 2017.